Dynamic susceptibility contrast and diffusion-weighted MRI in posterior fossa pilocytic astrocytoma and medulloblastoma

Short running title: DSC and DWI in posterior fossa tumors

Ryo Kurokawa[1,*], Yoshie Umemura[2], Aristides Capizzano[1], Mariko Kurokawa[1], Akira Baba[1], Adam Holmes[1], John Kim[1], Yoshiaki Ota[1], Ashok Srinivasan[1], Toshio Moritani[1]

1 Division of Neuroradiology, Department of Radiology, University of Michigan, Ann Arbor, Michigan

2 Department of Neurology in the University of Michigan Medical School, Ann Arbor, Michigan

*Corresponding Author:

Ryo Kurokawa

Division of Neuroradiology, Department of Radiology, University of Michigan, Ann Arbor, Michigan

1500 E Medical Center Dr, UH B2, Ann Arbor, MI 48109

Phone number: +1-734-219-2884

Fax number: +1-734-615-9800

Email address: kuroro63@gmail.com

Funding: none.

Keywords: pilocytic astrocytoma; medulloblastoma; dynamic susceptibility contrast; diffusion-weighted imaging; MRI

Abstract

Background and Purpose

The utility of perfusion MRI in distinguishing between pilocytic astrocytoma (PA) and medulloblastoma (MB) is unclear. This study aimed to evaluate the diagnostic and prognostic performance of dynamic susceptibility contrast (DSC)-MRI parameters and apparent diffusion coefficient (ADC) values between PA and MB.

Methods

Between January 2012 and August 2021, 49 (median, 7 years [range, 1–28 years]; 28 females) and 35 (median, 8 years [1–24 years]; 12 females) patients with pathologically confirmed PA and MB, respectively, were included. The normalized relative cerebral blood volume and flow (nrCBV and nrCBF) and mean and minimal normalized ADC (nADCmean and nADCmin) values were calculated

using volume-of-interest analyses. Diagnostic performance and Pearson's correlation with progression-free survival were also evaluated.

Results

The MB group showed a significantly higher nrCBV and nrCBF (nrCBV: 1.69 [0.93–4.23] vs. 0.95 [range, 0.37–2.28], p = 0.0032; nrCBF: 1.62 [0.93–3.16] vs. 1.07 [0.46–2.26], p = 0.0084) and significantly lower nADCmean and nADCmin (nADCmean: 0.97 [0.70–1.68] vs. 2.21 [1.44–2.80], p < 0.001; nADCmin: 0.50 [0.19–0.89] vs. 1.42 [0.89–2.20], p < 0.001) than the PA group. All parameters exhibited good diagnostic ability (accuracy >0.80) with nADCmin achieving the highest score (accuracy=1). A moderate correlation was found between nADCmean and progression-free survival for MB (r=0.44, p=0.0084).

Conclusions

DSC-MRI parameters and ADC values were useful for distinguishing between PA and MB. A lower ADC indicated an unfavorable MB prognosis, but the DSC-MRI parameters did not correlate with progression-free survival in either group.

Introduction

Brain tumors are the leading tumor-related cause of death in children,[1] with 45%–60% of pediatric brain tumors in the infratentorial regions.[2] Pilocytic astrocytoma (PA) and medulloblastoma (MB) are the most common tumors of the posterior cranial fossa.[2,3] PAs are low-grade (CNS World Health Organization [WHO] grade 1) tumors with a very high survival rate after diagnosis at most ages,[4] while MBs are classified as embryonal tumors with unfavorable outcomes if untreated (CNS WHO grade 4). Although the natural course of these two tumors is quite different, conventional MRI findings can be very similar, making differentiation through preoperative imaging challenging.

Significant efforts have been made to distinguish between these two tumors. Diffusion MRI techniques, including apparent diffusion coefficient (ADC) values/histograms[5–9] and diffusion tensor imaging,[10–12] MR spectroscopy,[13–15] and machine/deep learning,[16–18] have been the main foci of previous studies. However, reports on the diagnostic performance of perfusion MRI are scarce, with heterogeneous results. Duc demonstrated that relative cerebral blood flow (rCBF) derived from arterial spin labeling (ASL) was significantly higher in MB than in PA,[19] while Gupta et al. reported that dynamic contrast-enhanced (DCE)-MRI-derived rCBF and relative cerebral blood volume (rCBV) were significantly higher in PA than in MB.[20] Studies on dynamic susceptibility contrast (DSC)-MRI

are limited;[21,22] thus, the diagnostic performance in distinguishing PA and MB has not been established. Since perfusion parameters derived from different techniques are not necessarily comparable,[23] as indicated by the conflicting results of ASL and DCE studies, investigation and comparison of perfusion parameters using DSC-MRI in PA and MB are warranted. Furthermore, the rules for region-of-interest (ROI) placement and the handling of cysts, necrosis, hemorrhagic areas, and vasculature varied between the studies.

Another important role of MRI is its prognostication. The prognostic performance of perfusion MRI parameters (DSC and DCE) and ADC values has been documented in patients with newly diagnosed and recurrent glioblastomas.[24–28] As a prognostic factor from different viewpoints, Schob et al. reported that ADC histogram parameters were strongly correlated with the expression of the proliferation marker, Ki-67, and total nuclear area of MB.[29] However, for both PA and MB, the presence or absence of correlations between these MRI parameters and survival prognosis is unknown.

Therefore, this study aimed to evaluate the diagnostic and prognostic performance of DSC-MRI parameters and ADC values derived from volumes-of-interest (VOIs) in pediatric PA and MB in the posterior cranial fossa.

Methods

Institutional review board approval and consent exemptions were obtained. The data were acquired in compliance with all applicable Health Insurance Portability and Accountability Act regulations and were de-identified before any analysis.

Patients

Between January 2012 and August 2021, the electronic database of our hospital was searched, which yielded 55 and 40 patients with pathologically confirmed posterior fossa PA and MB, respectively, who underwent pretreatment brain MRI examinations. The inclusion and exclusion criteria were as follows.

- Inclusion criteria were pathologically proven PA and MB in the posterior fossa with pretreatment MRI, including diffusion-weighted imaging (DWI) and/or DSC-MRI.
- Exclusion criteria: age at diagnosis ≥ 30 years; strong artifact; intracranial leptomeningeal dissemination

Eight and five patients were excluded, respectively, due to the following reasons:

- PA group: age at diagnosis ≥30 years, n = 5; strong artifact, n = 3.

- MB group: age at diagnosis ≥30 years, n = 2; intracranial leptomeningeal dissemination, n = 2

Finally, 49 patients with PA and 35 patients with MB were included.

Demographic and clinical data

The following demographic and clinical data were collected: age at diagnosis, sex, treatment before the first progression, period between MRI and diagnosis, histological and molecular subgroups of MB, and progression-free survival (PFS) after diagnosis.

MRI scanning protocol

Brain MRI examinations were performed using 1T (n = 8), 1.5T (n = 52), and 3T (n = 24) MRI systems (Panorama HFO, Ingenia 1.5T, Ingenia 3T, Achieva: Philips Healthcare, Eindhoven; MAGNETOM Espree, MAGNETOM Vida: Siemens, Erlangen) with a 32-channel head coil in the supine position. The MRI acquisition protocols are summarized in Table 1. DSC-MRI was only performed using Ingenia 1.5T, Ingenia 3T, or MAGNETOM Vida (3T). For DSC-MRI, an intravenous bolus of 20 mL of gadobenate dimeglumine (Multihance, Bracco Diagnostics, Singen, Germany) or gadoteridol

(ProHance, Bracco Diagnostics, Inc., Princeton, NJ) was administered using a power injector via a peripheral arm vein at a flow rate of 5.0 mL/s, followed by a 20 mL saline flush. An additional 5 mL of contrast was administered 5 minutes before the dynamic perfusion scan. The parameters of fast field echo T2*-weighted imaging were as follows: dynamic measurements, 40; temporal resolution, 1.5 s; and total acquisition time, 1 min and 4.5 s. Steroids were given in five and four patients with PA and MB, respectively, within three months before the date of MRI examinations.

Quantitative DSC-MRI analyses

DSC-MRI was performed in 18 and 13 patients with PA and MB, respectively. Quantitative DSC-MRI analyses were conducted using OleaSphere (Version 3.0; Olea Medical, La Ciotat, France). The DSC-MRI data were processed with motion artifact correction using rigid-body registration. The arterial input function (AIF) was calculated automatically using cluster analysis techniques, and deconvolution of the AIF was performed with time-insensitive block-circulant singular-value decomposition.[30] Whole-brain rCBV and rCBF maps were generated using voxel-wise division of the area under the concentration-time curve by the area under the AIF. A board-certified radiologist with 9 years of experience in neuroradiology carefully delineated the ROIs freehand on each axial slice of the perfusion maps depicting the tumor to generate the VOIs while excluding cystic, necrotic,

or hemorrhagic regions and vessels using reference T2-weighted, fluid-attenuated inversion recovery, pre-and post-contrast T1-weighted, and T2*-weighted images under the direct supervision of another board-certified radiologist with 13 years of experience in neuroradiology. Another ROI was placed over the normal-appearing white matter as a reference to correct for age- and patient-dependent variations in perfusion parameters.[31] The VOI and reference ROI on perfusion maps were transposed to the corrected rCBV and rCBF maps. Finally, the normalized rCBV (nrCBV) and normalized rCBF (nrCBF) were calculated by dividing the mean rCBV and mean rCBF of the tumor by that of the reference ROIs.

Quantitative ADC analyses

DWI was performed for all patients with PA and MB. ADC maps were generated using OleaSphere. Three orthogonal orientations were used for ADC estimation, and is also rotationally-invariant. The VOIs were generated on the solid components of the tumors using the same method as that used for DSC-MRI analysis. A reference ROI was placed in normal-appearing white matter. The normalized mean ADC (nADCmean) and normalized minimal ADC (nADCmin) were calculated for each VOI of the tumors by dividing the ADC values by the mean ADC of the reference ROIs.

Statistical analysis

Age, follow-up period (months), PFS, OS, DSC-MRI parameters (nrCBV and nrCBF), and ADC values (nADCmean and nADCmin) were compared between the two tumor groups using the Mann-Whitney U test or t-test as appropriate, based on the results of the Shapiro-Wilk test. nrCBV, nrCBF, nADCmean, and nADCmin were also compared between molecular subtypes of MB using the Mann-Whitney U test or t-test as appropriate. Sex, disease progression, and living status were compared between the groups using Fisher's exact test. The diagnostic performance, sensitivity, specificity, positive predictive value, negative predictive value, accuracy, and area under the receiver operator characteristic curve (AUC) of each MRI parameter for distinguishing MB from PA were calculated using the optimal cutoff values to distinguish MB from PA as determined by the highest Youden index (sensitivity + specificity -1).[32] Pearson's correlation analysis was performed to determine the association between each MRI parameter and PFS for each tumor group. The strength of the correlation was interpreted as very weak (|r| = ≤0.20), weak (|r| = 0.21–0.39), moderate (|r| = 0.40–0.59), strong (|r| = 0.60–0.79), and very strong (|r| = ≥0.80). [33] Two-sided P values of <0.01 were considered statistically significant. All statistical analyses were performed using R (version 4.0.0; R Foundation for Statistical Computing, Vienna, Austria).

Results

Patients

The demographic, clinical, and radiological data are summarized in Table 2 and Table 3. The study participants consisted of 49 patients with PA (median 7 years [range 1–28 years]; 28 females) and 35 patients with MB (median 8 years [1–24 years]; 12 females). DSC-MRI was performed in 18 patients with PA (median 9 years [2–26 years]; 9 females) and 13 patients with MB (median 10 years [1–24 years]; 3 females).

Diagnostic performance of MRI parameters

The MB group showed a significantly higher nrCBV and nrCBF (nrCBV: 1.69 [0.93–4.23] vs. 0.95 [range, 0.37–2.28], p = 0.0032; nrCBF: 1.62 [0.93–3.16] vs. 1.07 [0.46–2.26], p = 0.0084) and significantly lower nADCmean and nADCmin (nADCmean: 0.97 [0.70–1.68] vs. 2.21 [1.44–2.80], p < 0.001; nADCmin: 0.50 [0.19–0.89] vs. 1.42 [0.89–2.20], p < 0.001) than the PA group (Fig. 1 and Fig. 2). Both DSC-MRI parameters and ADC values showed high diagnostic performance with an accuracy score of >0.80 (Table 4). The nADCmin achieved the highest accuracy score for differentiating MB

from PA (accuracy = 1). Representative MR images of patients with PA and MB are shown in Fig. 3 and Fig. 4, respectively.

Correlation between MRI parameters and PFS

There was a moderately significant correlation between nADCmean and PFS for MB (r = 0.44, p = 0.0084) (Table 5). However, no significant correlation was found between MRI parameters and PFS for PA.

Discussion

In this study, the DSC-MRI parameters and ADC values were compared between PA and MB. The nrCBV and nrCBV were significantly higher, while nADCmean and nADCmin were significantly lower in MB than in PA. All of the investigated parameters demonstrated remarkable diagnostic performance with high accuracy, particularly nADCmin, which exhibited perfect distinguishing ability using a cutoff value of 0.893. The nADCmean also showed a moderate correlation with PFS for MB, but no significant correlation was found between MRI parameters and PFS for PA.

Given the quite differences in the natural course, required analyses, and surgical approaches between PA and MB, the differentiation of these two tumor types by neuroimaging is very important. PAs are CNS WHO grade 1 tumors with favorable outcomes,[4] while MBs are CNS WHO grade 4 tumors with unfavorable outcomes if untreated. Surgical resection and "wait and see" approach may be followed in young patients with PA,[34] while surgical resection of the primary mass, craniospinal radiation therapy, and chemotherapy are generally performed in those with MB.[35] Additionally, both brain and spine MRI and cerebrospinal fluid cytology should be assessed for MB.[35]

The differentiation of PA and MB using ADC values has been previously reported.[5–9] Although the types (e.g., mean and/or minimum ADC, variance, skewness, kurtosis, and percentiles) and measurement methods (subjective signal intensity or objective values derived from either 2D-ROI or 3D-VOI) of ADC values were not homogeneous in these studies, in general, these studies reported the high diagnostic ability of ADC values to differentiate the two tumors. Phuttharak et al. reported that an ADC ratio of ≤1.17 between the mean lowest ADC value derived from three different ROIs within the tumor to normal cerebellar white matter demonstrated a sensitivity, specificity, positive predictive value, negative predictive value, and AUC of 0.958, 1.0, 1.0, 0.929, and 0.9936, respectively,[5] which were similar to those of the current study. Yamashita et al. evaluated the minimal ADC among posterior fossa tumors and found a significantly lower minimal ADC in MB

than in PA, which was also consistent with the present study.[9] The clear difference in ADC values between PA and MB may be explained by the different histopathological characteristics of these tumors. MB typically shows densely packed cells with hyperchromatic nuclei and minimal cytoplasm.[36] In contrast, PA is a tumor with low to moderate cellularity with varying degrees of mucoid background material and microcyst development,[37] which may explain the tendency toward high ADC values.

Our current understanding of the diagnostic performance of perfusion MRI techniques in PA and MB is limited. Duc demonstrated that the rCBF derived from ASL was significantly higher in MB than in PA with a sensitivity of 0.88, specificity of 0.75, and an AUC of 0.835 using a cutoff value of 0.51.[19] Interestingly, these diagnostic values were similar to the results found in this study (sensitivity 0.85, specificity 0.76, and AUC, 0.81). The lower blood flow/volume in PA than in higher-grade tumors is also in line with studies comparing perfusion parameters between PA and high-grade gliomas.[38–40] In contrast, Gupta et al. reported significantly lower rCBV and rCBF in MB than in PA in their DCE-MRI study.[20] The discrepancy between the results of perfusion studies in PA, including the present study, may be partially attributable to the variety of angiogenic profiles in PA, such as microvessel density and vessel stability.[41] Differences in perfusion techniques are another

potential explanation.[23] Moreover, the different rules in the ROI placement may have affected the results in each study. How ROIs were placed and how cysts, necrosis, hemorrhagic areas, and vasculature were handled were not detailed in the study by Duc et al.;[19] vasculature was avoided but ROIs were placed on the region of the tumor with the highest value of each perfusion metric in the study by Gupta et al.[20] Although the results of subgroup analyses for the molecular subtypes in patients with MB did not reach significance, there were tendencies that MRI parameters were different between the molecular subtypes (Table 3). Given the small number of the patients with each subtype, future studies are warranted to evaluate the MRI features of each molecular subtypes.

Regarding prognostication performance, a moderate positive correlation was found between nADCmean and PFS in patients with MB. To the best of our knowledge, this is the first study to demonstrate this correlation. There have been several reports indicating a correlation between lower ADC values and higher proliferation ability and consequently increased chromatin content in the tumor cells of MB.[9,29,42] In contrast, no significant correlation was demonstrated with DSC or between ADC values and PFS in patients with PA. Several mechanisms may be responsible, including the variety of histological characteristics of PA, as described above. While high tumor

perfusion parameters generally suggest an environment conducive to tumor growth, improved tumor perfusion also provides the opportunity to better respond to treatment by increasing the delivered chemotherapeutics to the tumor and improving the radiation effect by reducing hypoxia.[43,44] Therefore, the effect of perfusion on prognosis may be complicated by the association with treatment responsiveness or resistance, and thus a one-size-fits-all approach may not be appropriate. However, the role of DSC-MRI parameters in pediatric posterior fossa tumors as a measure of the response to treatment and in the detection of tumor progression is an important topic for future research.

This study had some limitations. First, this was a single institutional retrospective study, and not all patients underwent DSC-MRI, which might have led to insufficient analysis of DSC-MRI parameters. Second, MRI protocols were not homogeneous owing to differences in machines and vendors. However, we mitigated the risk of heterogeneity of MRI parameters by normalization. Third, steroids were given in five and four patients with PA and MB, respectively, before the date of MRI examinations. This might have affected the quantitative values of the data. Fourth, the molecular subgroup was unknown in some patients with MB. Therefore, subgroup-specific analyses were not possible. Further studies with molecularly diagnosed MB are required. Finally, the

follow-up period varied from 3–4 months to several years, which might have affected the survival outcomes, although no significant difference was found between the two tumor groups.

In conclusion, the nrCBV and nrCBF were significantly higher and the nADCmean and nADCmin were significantly lower in patients with MB than in those with PA. The MRI parameters, particularly the ADC values, demonstrated a remarkable diagnostic performance with high accuracy. The nADCmean showed a moderate correlation with PFS for MB, indicating that a lower ADC was associated with unfavorable tumor behavior, but the DSC-MRI parameters did not correlate with PFS in either tumor group.

Acknowledgements and Disclosure

We would like to thank Editage [http://www.editage.com] for editing and reviewing this manuscript for English language.

The authors declare that they have no competing interests.

Reference

1. Ostrom QT, Patil N, Cioffi G, et al. CBTRUS statistical report: primary brain and other central nervous system tumors diagnosed in the United States in 2013-2017. Neuro Oncol 2020;22:iv1–iv96.

2. Poretti A, Meoded A, Huisman TAGM. Neuroimaging of pediatric posterior fossa tumors including review of the literature. J Magn Reson Imaging 2012;35:32–47.

3. Koeller KK, Rushing EJ. From the archives of the AFIP: pilocytic astrocytoma: radiologic-pathologic correlation. Radiographics 2004;24:1693-708.

4. Ostrom QT, Kruchko C, Barnholtz-Sloan JS. Pilocytic astrocytomas: where do they belong in cancer reporting? Neuro Oncol 2020;22:298–300.

5. Phuttharak W, Wannasarnmetha M, Wara-Asawapati S, Yuthawong S. Diffusion MRI in evaluation of pediatric posterior fossa tumors. Asian Pac J Cancer Prev 2021;22:1129–36.

6. Duc NM, Huy HQ. Magnetic resonance imaging features of common posterior fossa brain tumors in children: a preliminary Vietnamese study. Open Access Maced J Med Sci 2019;7:2413–18.

7. Wang W, Cheng J, Zhang Y, Wang C. Use of apparent diffusion coefficient histogram in differentiating between medulloblastoma and pilocytic astrocytoma in children. Med Sci Monit 2018;24:6107–12.

8. Rodriguez Gutierrez D, Awwad A, Meijer L, et al. Metrics and textural features of MRI diffusion to improve classification of pediatric posterior fossa tumors. AJNR Am J Neuroradiol 2014;35:1009–15.

9. Yamashita Y, Kumabe T, Higano S, et al. Minimum apparent diffusion coefficient is significantly correlated with cellularity in medulloblastomas. Neurol Res 2009;31:940–6.

10. Minh Duc N. The performance of diffusion tensor imaging parameters for the distinction between medulloblastoma and pilocytic astrocytoma. Minerva Pediatr (Torino) 2021 [Epub ahead of print]

11. Wagner MW, Narayan AK, Bosemani T, et al. Histogram analysis of diffusion tensor imaging parameters in pediatric cerebellar tumors. J Neuroimaging 2016;26:360–5.

12. Assis ZA, Saini J, Ranjan M, et al. Diffusion tensor imaging in evaluation of posterior fossa tumors in children on a 3T MRI scanner. Indian J Radiol Imaging 2015;25:445–52.

13. Manias KA, Harris LM, Davies NP, et al. Prospective multicentre evaluation and refinement of an analysis tool for magnetic resonance spectroscopy of childhood cerebellar tumours. Pediatr Radiol 2018;48:1630–41.

14. Zarinabad N, Wilson M, Gill SK, et al. Multiclass imbalance learning: improving classification of pediatric brain tumors from magnetic resonance spectroscopy. Magn Reson Med 2017;77:2114–24.

15. Raschke F, Davies NP, Wilson M, et al. Classification of single-voxel 1H spectra of childhood cerebellar tumors using LCModel and whole tissue representations. Magn Reson Med 2013;70:1–6.

16. Zhou H, Hu R, Tang O, et al. Automatic machine learning to differentiate pediatric posterior fossa tumors on routine MR imaging. AJNR Am J Neuroradiol 2020;41:1279–85.

17. Zhang M, Wong SW, Wright JN, et al. Machine assist for pediatric posterior fossa tumor diagnosis: a multinational study. Neurosurgery 2021;89:892–900.

18. Quon JL, Bala W, Chen LC, et al. Deep learning for pediatric posterior fossa tumor detection and classification: a multi-institutional study. AJNR Am J Neuroradiol 2020;41:1718–25.

19. Duc NM. Three-dimensional pseudo-continuous arterial spin labeling parameters distinguish pediatric medulloblastoma and pilocytic astrocytoma. Front Pediatr 2020;8:598190.

20. Gupta PK, Saini J, Sahoo P, et al. Role of dynamic contrast-enhanced perfusion magnetic resonance imaging in grading of pediatric brain tumors on 3T. Pediatr Neurosurg 2017;52:298–305.

21. Novak J, Withey SB, Lateef S, et al. A comparison of pseudo-continuous arterial spin labelling and dynamic susceptibility contrast MRI with and without contrast agent leakage correction in paediatric brain tumours. Br J Radiol 2019;92:20170872.

22. Testud B, Brun G, Varoquaux A, et al. Perfusion-weighted techniques in MRI grading of pediatric cerebral tumors: efficiency of dynamic susceptibility contrast and arterial spin labeling. Neuroradiology 2021;63:1353–66.

23. Lüdemann L, Warmuth C, Plotkin M, et al. Brain tumor perfusion: comparison of dynamic contrast enhanced magnetic resonance imaging using T1, T2, and T2* contrast, pulsed arterial spin labeling, and H2(15)O positron emission tomography. Eur J Radiol 2009;70:465–74.

24. Wirsching H-G, Roelcke U, Weller J, et al. MRI and 18FET-PET predict survival benefit from bevacizumab plus radiotherapy in patients with isocitrate dehydrogenase wild-type glioblastoma: results from the randomized ARTE trial. Clin Cancer Res 2021;27:179–88.

25. Omuro A, Beal K, Gutin P, et al. Phase II study of bevacizumab, temozolomide, and hypofractionated stereotactic radiotherapy for newly diagnosed glioblastoma. Clin Cancer Res 2014;20:5023–31.

26. Pope WB, Lai A, Mehta R, et al. Apparent diffusion coefficient histogram analysis stratifies progression-free survival in newly diagnosed bevacizumab-treated glioblastoma. AJNR Am J Neuroradiol 2011;32:882–9.

27. Choi SH, Jung SC, Kim KW, et al. Perfusion MRI as the predictive/prognostic and pharmacodynamic biomarkers in recurrent malignant glioma treated with bevacizumab: a systematic review and a time-to-event meta-analysis. J Neurooncol 2016;128:185–94.

28. Kickingereder P, Wiestler B, Burth S, et al. Relative cerebral blood volume is a potential predictive imaging biomarker of bevacizumab efficacy in recurrent glioblastoma. Neuro Oncol 2015;17:1139–47.

29. Schob S, Beeskow A, Dieckow J, et al. Diffusion profiling of tumor volumes using a histogram approach can predict proliferation and further microarchitectural features in medulloblastoma. Childs Nerv Syst 2018;34:1651–6.

30. Mouridsen K, Christensen S, Gyldensted L, Ostergaard L. Automatic selection of arterial input function using cluster analysis. Magn Reson Med 2006;55:524–31.

31. Morana G, Tortora D, Staglianò S, et al. Pediatric astrocytic tumor grading: comparison between arterial spin labeling and dynamic susceptibility contrast MRI perfusion. Neuroradiology 2018;60:437–46.

32. Youden WJ. Index for rating diagnostic tests. Cancer 1950;3:32–5.

33. Evans JD. Straightforward statistics for the behavioral sciences. Brooks/Cole Publishing Company; 1996.

34. Sepúlveda-Sánchez JM, Muñoz Langa J, Arráez MÁ, Fuster J, Hernández Laín A, Reynés G, et al. SEOM clinical guideline of diagnosis and management of low-grade glioma. Clin Transl Oncol 2018;20:3–15.

35. Warren KE, Vezina G, Poussaint TY, Warmuth-Metz M, Chamberlain MC, Packer RJ, et al. Response assessment in medulloblastoma and leptomeningeal seeding tumors: recommendations from the Response Assessment in Pediatric Neuro-Oncology committee. Neuro Oncol 2018;20:13–23.

36. Orr BA. Pathology, diagnostics, and classification of medulloblastoma. Brain Pathol 2020;30:664–78.

37. Collins VP, Jones DTW, Giannini C. Pilocytic astrocytoma: pathology, molecular mechanisms and markers. Acta Neuropathol 2015;129:775–88.

38. de Fatima Vasco Aragao M, Law M, Batista de Almeida D, et al. Comparison of perfusion, diffusion, and MR spectroscopy between low-grade enhancing pilocytic astrocytomas and high-grade astrocytomas. AJNR Am J Neuroradiol 2014;35:1495–502.

39. Dangouloff-Ros V, Deroulers C, Foissac F, et al. Arterial spin labeling to predict brain tumor grading in children: correlations between histopathologic vascular density and perfusion MR imaging. Radiology 2016;281:553–66.

40. Kikuchi K, Hiwatashi A, Togao O, et al. Usefulness of perfusion- and diffusion-weighted imaging to differentiate between pilocytic astrocytomas and high-grade gliomas: a multicenter study in Japan. Neuroradiology 2018;60:391–401.

41. Sie M, de Bont ESJM, Scherpen FJG, et al. Tumour vasculature and angiogenic profile of paediatric pilocytic astrocytoma; is it much different from glioblastoma? Neuropathol Appl Neurobiol 2010;36:636–47.

42. Reis J, Stahl R, Zimmermann H, et al. Advanced MRI findings in medulloblastomas: relationship to genetic subtypes, histopathology, and immunohistochemistry. J Neuroimaging 2021;31:306–16.

43. Batchelor TT, Gerstner ER, Emblem KE, et al. Improved tumor oxygenation and survival in glioblastoma patients who show increased blood perfusion after cediranib and chemoradiation. Proc Natl Acad Sci U S A 2013;110:19059–64.

44. Rockwell S, Dobrucki IT, Kim EY, et al. Hypoxia and radiation therapy: past history, ongoing research, and future promise. Curr Mol Med 2009;9:442–58.

Tables

Table 1. MRI acquisition protocol

	T2WI	FLAIR	Pre-and Post-contrast fat-sat T1WI	DWI (b= 0, 1000 s/mm^2)
Plane	Axial	Axial	Axial	Axial
Repetitive time (ms)	3930–5906	8500–11000	500–2300	3529–5960
Echo time (ms)	80–110	105–140	5–20	58.2–91.2
Flip angle (degree)	90–135	90–150	69–125	90–180
Number of excitations	1–3	1, 2	1,2	1,2
Slice thickness / increment (mm)	4–5/4.4–6	4–5/4.4–6	4–5/4.4–6	4–5/4.4–5
Field of view (mm)	227–236	228–252	160–240	227–251
Matrix	224 × 224 – 560 × 560	320 × 310 – 560 × 560	188 × 188–320 × 320	176 × 176–320 × 320

T2WI, T2-weighted imaging; FLAIR, Fluid-attenuated inversion recovery; T1WI, T1-weighted imaging; DWI, Diffusion-w
T2*WI, T2*-weighted imaging

Table 2. Demographic, clinical, and radiological data

	Medulloblastoma (MB)		Pilocytic astrocytoma (PA)		P-value	
	All (35 patients)	with DSC examination (13 patients)	All (49 patients)	with DSC examination (18 patients)	All MB vs. All	M B w it

					PA vs. PA with hDSC	hDSC vs. PA with hDSC
Demographic and clinical data						
Age (median, range)	8 years (1–24)	10 years (1–24)	7 years (1–28)	9 years (2–26)	0.93	0.87
Sex (male: female)	23: 12	10: 3	21: 28	9: 9	0.032*	0.13
MB, histopathologic subtypes						
Classic	22	10				
Large	5	1				

cell/anaplastic				
Desmoplastic/nodular	0	0		
Unknown	8	2		
MB, molecular subtypes				
WNT-activated	4	4		
SHH-activated and TP53-wildtype	2	1		
SHH-activated and TP53-mutant	1	0		
SHH-activated with unknown TP53 status	3	2		
Non-WNT/non-SHH	9	6		
Unknown	17	0		
PA, BRAF mutation status				
BRAF V600E/K			0/20	0/5
KIAA-BRAF fusion			27/30	10/11
Treatment before the first progression				

Surgery	35 (100%)	13 (100%)	49 (100%)	18 (100%)		
Chemotherapy	33 (94.3%)	11 (84.6%)	2 (4.1%)	0		
Radiation	31 (88.6%)	11 (84.6%)	0	0		
Bone marrow transplantation	3 (8.6%)	2 (15.4%)	0	0		
Progression of disease (absence: presence)	25: 10	10: 3	44: 5	15: 3	0.031*	0.50
Survival status (survived: deceased)	27: 8	12: 1	49: 0	18: 0	<0.001**	0.42
Follow-up period (median, range)	47 months (4–112)	29 months (4–73)	36 months (3–110)	44 months (6–110)	0.72	0.31
Progression-free survival (median, range)	27 months (<1–107)	23 months (3–71)	29 months (2–101)	22 months (2–88)	0.98	0.80
Radiological data (median, range)						
nrCBV	1.69 (0.93–4.23)		0.95 (0.37–2.28)		0.0032**	
nrCBF	1.62 (0.93–3.16)		1.07 (0.46–2.26)		0.0084**	

nADCmean	0.97 (0.70–1.68)	2.21 (1.44–2.80)	<0.001** *
nADCmin	0.50 (0.19–0.89)	1.42 (0.89–2.20)	<0.001** *

* p < 0.05; ** p < 0.01; *** p < 0.001

MB, medulloblastoma; PA, pilocytic astrocytoma; DSC, dynamic susceptibility contrast; nrCBV/F, normalized relative cerebral blood volume/flow; nADCmean/min, mean/minimum normalized apparent diffusion coefficient

. Subgroup analyses

	WNT-activated (Medulloblastoma)	SHH-activated (Medulloblastoma)	non-WNT/non-SHH (Medulloblastoma)
nrCBV	Positive (3 patients): 2.71 [2.66–2.91] Negative (9 patients): 1.60 [0.93–4.23] p = 0.052	Positive (3 patients): 1.49 [0.94–2.27] Negative (9 patients): 1.73 [0.93–4.23] p = 0.31	Positive (6 patients): 1.64 [0.93–4.23] Negative (6 patients): 2.47 [0.94–2.91] p = 0.42
nrCBF	Positive (3 patients): 2.65 [1.37–2.76] Negative (9 patients): 1.39 [0.93–3.16] p = 0.31	Positive (3 patients): 1.37 [0.93–2.40] Negative (9 patients): 1.68 [1.10–3.16] p = 0.41	Positive (6 patients): 1.54 [1.10–3.16] Negative (6 patients): 1.89 [0.93–2.76] p = 0.87
nADCmean	Positive (3 patients): 0.91 [0.82–0.93] Negative (15 patients):	Positive (5 patients): 0.83 [0.70–1.37] Negative (13 patients):	Positive (10 patients): 0.99 [0.92–1.26] Negative (8 patients): 0.97

	0.98 [0.70–1.68]	0.97 [0.76–1.68]	[0.70–1.68]
	p = 0.14	p = 0.26	p = 0.033*
	Positive (3 patients): 0.27 [0.20–0.37]	Positive (5 patients): 0.44 [0.32–0.70]	Positive (10 patients): 0.54 [0.37–0.69]
	Negative (15 patients):	Negative (13 patients):	Negative (8 patients): 0.48
nADCm	0.51 [0.19–0.89]	0.50 [0.19–0.89]	[0.19–0.89]
in	p = 0.015*	p = 0.73	p = 0.13

* $p < 0.05$

Values: median [range]

nrCBV/F normalized relative cerebral blood volume/flow; nADCmean/min, mean/minimum normalized apparent diffusion coefficient

Table 4. Diagnostic performance of DSC-MRI parameters and ADC values

Cutoff value*	nrCBV ≥ 1.40	nrCBF ≥ 1.25	nADCmean < 1.44	nADCmin < 0.893
Sensitivity	0.77	0.85	0.97	1
Specificity	0.82	0.76	1	1
Positive predictive value	0.77	0.73	1	1
Negative predictive value	0.82	0.87	0.98	1
Accuracy	0.80	0.80	0.99	1
AUC	0.83	0.81	0.998	1

*Cutoff values to distinguish medulloblastoma from pilocytic astrocytoma.

DSC, dynamic susceptibility contrast; nrCBV/F, normalized relative cerebral blood volume/flow; nADCmean/min, mean/minimum normalized apparent diffusion coefficient; AUC, area under the receiver operator characteristic curve

This is the author manuscript accepted for publication and has undergone full peer review but has not been through the copyediting, typesetting, pagination and proofreading process, which may lead to differences between this version and the Version of Record. Please cite this article as doi: 10.1111/jon.12962_org.

Table 5. Correlation between MRI parameters and progression-free survival

	Pilocytic astrocytoma	Medulloblastoma
nrCBV	r = -0.069, p = 0.78	r = 0.25, p = 0.41
nrCBF	r = 0.13, p = 0.59	r = 0.38, p = 0.20
nADCmean	r = -0.055, p = 0.71	r = 0.44, p = 0.0084*
nADCmin	r = 0.18, p = 0.22	r = 0.23, p = 0.18

* Statistically significant

nrCBV/F, normalized relative cerebral blood volume/flow; nADCmean/min, mean/minimum normalized apparent diffusion coefficient

Figure Legends

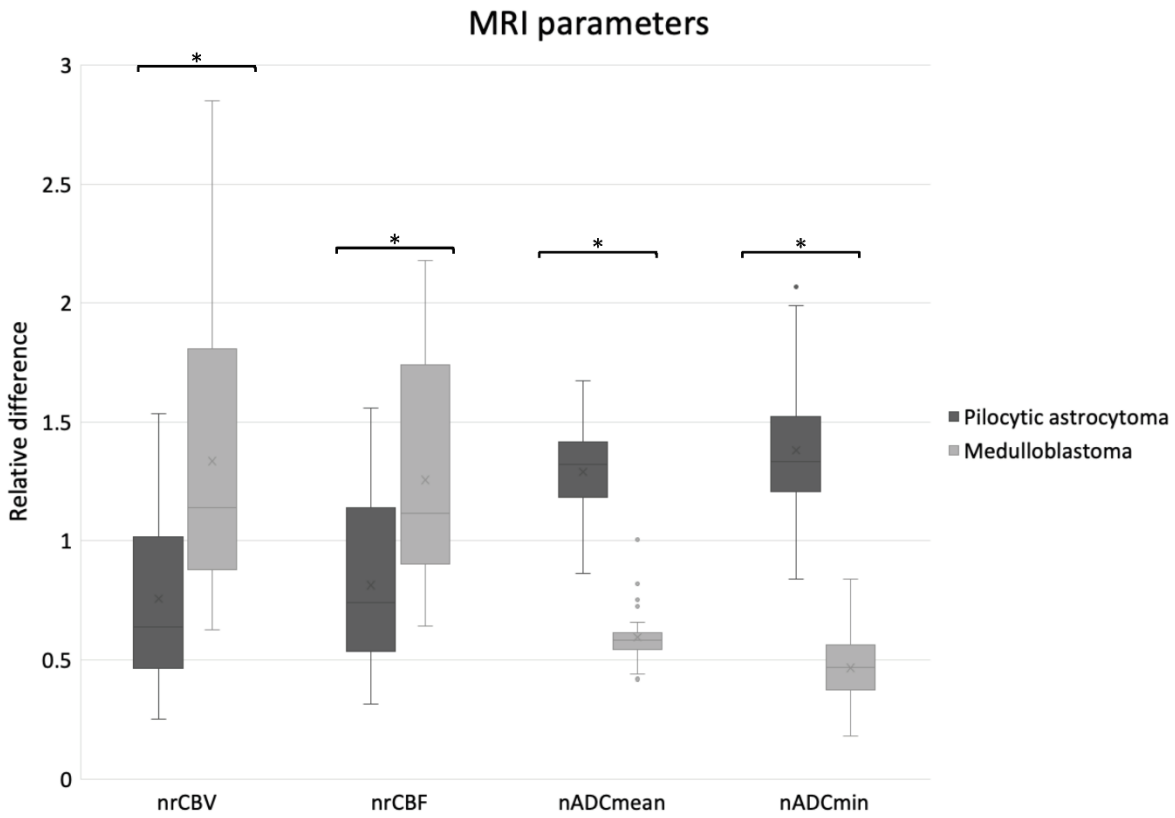

Figure 1. Differences in magnetic resonance imaging parameters relative to the cross-tumor mean. Boxplots represent the median and interquartile ranges for all patients. Cross-marks represent mean. * Statistically significant. nrCBV/F, normalized relative cerebral blood volume/flow; nADCmean/min, mean/minimum normalized apparent diffusion coefficient

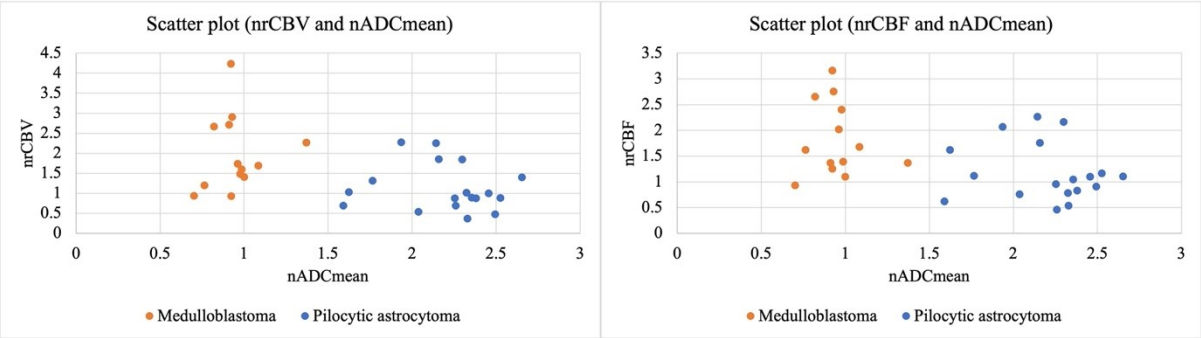

Figure 2. Scatterplots of normalized mean ADC (nADCmean) and normalized relative cerebral blood volume (nrCBV) and flow (nrCBF).

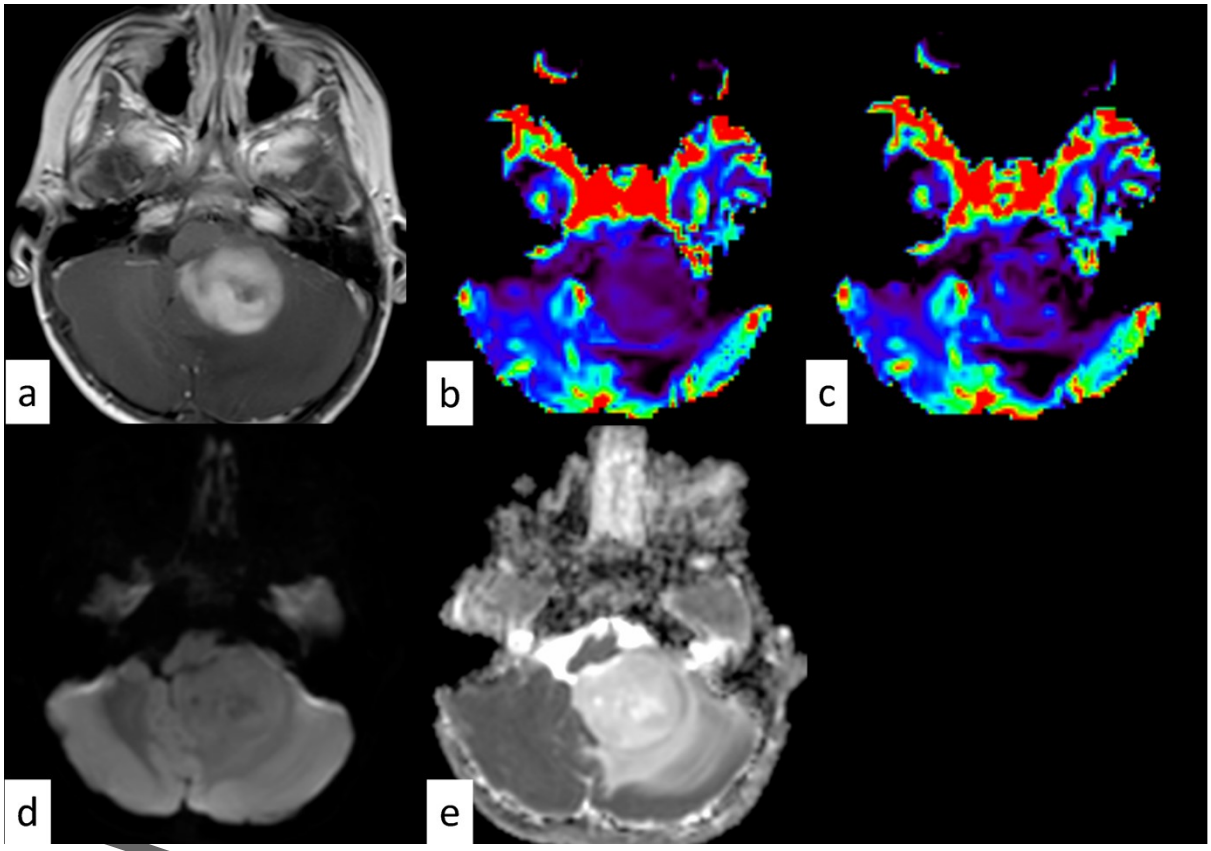

Figure 3. Pilocytic astrocytoma in a 2-year-old girl. Magnetic resonance imaging showed a mass with cystic change in the cerebellum, causing hydrocephalus (not shown). The tumor shows heterogeneous enhancement on post-contrast T1-weighted imaging (a) without an elevated normalized relative cerebral blood volume (b, 0.53) or normalized relative cerebral blood flow (c, 0.76). The tumor shows intermediate intensity on diffusion-weighted imaging (d) with a high mean normalized apparent diffusion coefficient (2.04) and minimum normalized apparent diffusion coefficient (1.45) (e). The tumor was resected but recurred 5 months later.

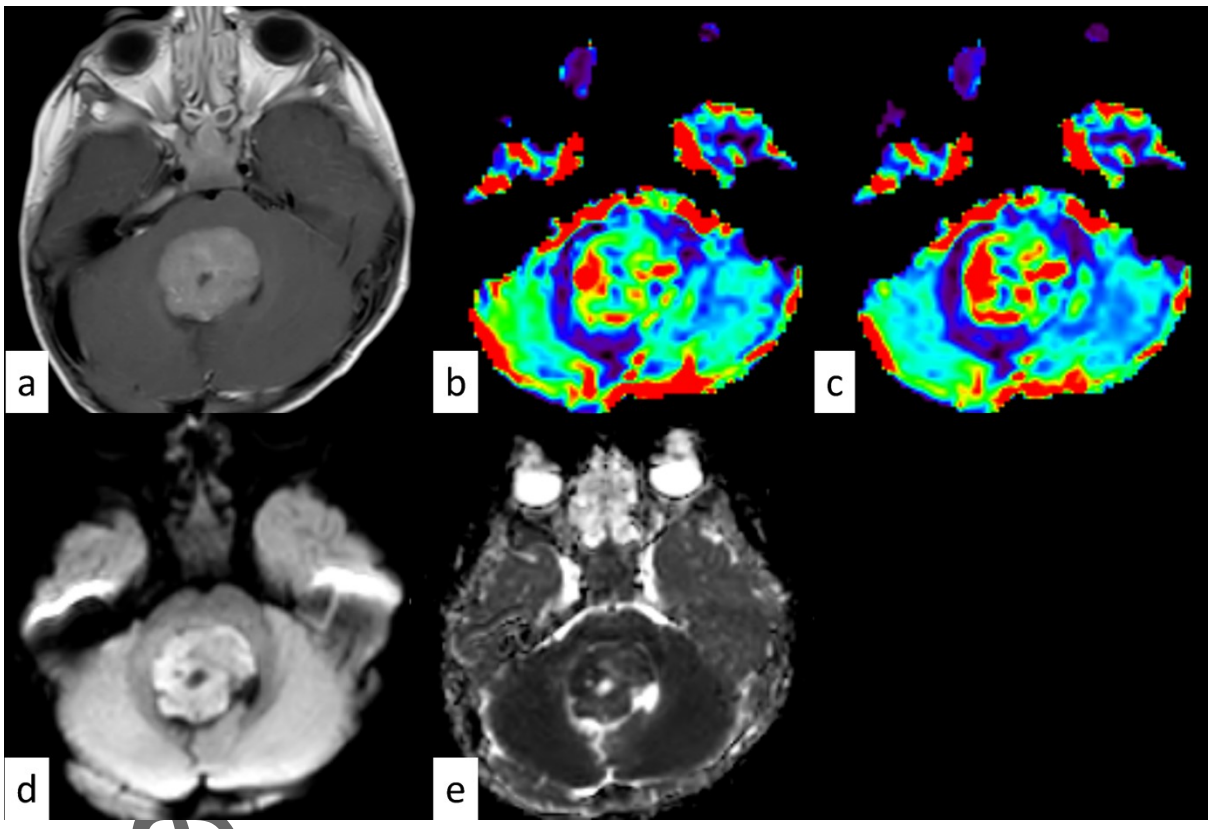

Figure 4. Medulloblastoma (classic, SHH-activated and TP53-wildtype) in a 1-year-old girl.

Magnetic resonance imaging showed a mass with cystic change in the floor of the fourth ventricle causing hydrocephalus (not shown). The tumor shows heterogeneous enhancement on post-contrast T1-weighted imaging (a) with an elevated normalized relative cerebral blood volume (b, 1.49) and normalized relative cerebral blood flow (c, 2.40). The tumor shows high intensity on diffusion-weighted imaging (d) with a low mean normalized apparent diffusion coefficient (0.98) and minimum normalized apparent diffusion coefficient (0.65) (e). The patient underwent surgery followed by autologous hematopoietic stem cell transplantation. The patient has been treatment free for more than 2 years without recurrence.